Biophysical Journal
Article

Biophysical Society

# Search and Capture Efficiency of Dynamic Microtubules for Centrosome Relocation during IS Formation

Apurba Sarkar,[1,*] Heiko Rieger,[2,*] and Raja Paul[1,*]
[1]School of Mathematical & Computational Sciences, Indian Association for the Cultivation of Science, Kolkata, West Bengal, India and
[2]Department of Theoretical Physics and Center for Biophysics, Saarland University, Saarbrücken, Germany

ABSTRACT Upon contact with antigen-presenting cells, cytotoxic T lymphocytes (T cells) establish a highly organized contact zone denoted as the immunological synapse (IS). The formation of the IS implies relocation of the microtubule organizing center (MTOC) toward the contact zone, which necessitates a proper connection between the MTOC and the IS via dynamic microtubules (MTs). The efficiency of the MTs finding the IS within the relevant timescale is, however, still illusive. We investigate how MTs search the three-dimensional constrained cellular volume for the IS and bind upon encounter to dynein anchored at the IS cortex. The search efficiency is estimated by calculating the time required for the MTs to reach the dynein-enriched region of the IS. In this study, we develop simple mathematical and numerical models incorporating relevant components of a cell and propose an optimal search strategy. Using the mathematical model, we have quantified the average search time for a wide range of model parameters and proposed an optimized set of values leading to the minimal capture time. Our results show that search times are minimal when the IS formed at the nearest or at the farthest sites on the cell surface with respect to the perinuclear MTOC. The search time increases monotonically away from these two specific sites and is maximal at an intermediate position near the equator of the cell. We observed that search time strongly depends on the number of searching MTs and distance of the MTOC from the nuclear surface.

## INTRODUCTION

Cytotoxic T lymphocytes (T cells) play a crucial role in adaptive immunity by defending against virus-infected and tumorigenic cells. Directional killing of an antigen-presenting cell (APC) by T cells is completed in multiple steps, including 1) binding of the T cell receptor to the cognate antigen presented by the major histocompatibility complex on the surface of the APC. The interaction leads to the formation of a specialized T cell/APC junction denoted as the immunological synapse (IS), consisting of several supramolecular activation clusters (1–4); 2) establishment of the connection between the T cell's centrosome or microtubule organizing center (MTOC) and the synapse by the dynamic microtubules (MTs) (5,6); 3) translocation of the MTOC to or near the target contact site achieved by the development of tension on MTs (5,7,8); and 4) the subsequent secretion of the cytotoxic content of lytic vesicles at the IS via exocytosis, which kills the target cell (9–12).

Immediately after the establishment of the IS, the T cell's MTOC moves to a position that is just underneath the plasma membrane at the center of the IS (9,13,14). One important consequence of MTOC relocation in T cells is that the MT minus-end-directed transport of vesicles containing cytotoxic material can be directed toward and terminated immediately adjacent to the bound APC for subsequent secretion via exocytosis (9–12). In search of understanding MTOC translocation toward the synapse, suggested by Geiger et al. (13), modulated polarization microscopy facilitated the visualization of the cytoskeleton and MTOC in living cells (8,15). Modulated polarization microscopy studies revealed that MTOC repositioning is associated with a development of tension on the MTs, resulting in a pulling on the MTOC toward the IS. Before the initiation of the MTOC relocation, the MTs are seen to be nucleated from the MTOC, curve spontaneously following the shape of the cell boundary contacting the IS (8). It is suggested that actin polymerizing in a small patch at the center of the IS may facilitate MTs to connect through IQGAP or CIP4 proteins (14,16–20). During

*Submitted February 25, 2019, and accepted for publication April 8, 2019.*
*Correspondence: sspas2@iacs.res.in or h.rieger@mx.uni-saarland.de or raja.paul@iacs.res.in
Editor: Stefan Diez.
https://doi.org/10.1016/j.bpj.2019.04.008

the development of the IS, actin clears out from the center of the synapse. As actin spreads out in the form of an expanding ring, tension develops on the MTs as the ring enlarges (14,21). The MT-associated molecular motor protein dynein assists this tension development on the MTs, and it has been suggested that dyneins drive the MTOC toward the IS via cortical sliding (8,22,23).

A quantitative theoretical model for MTOC relocation based on the "cortical sliding" mechanism has been suggested by Kim and Maly (24). According to the proposed model, the T cell is represented by a sphere with a radius of 5–10 $\mu$m that forces the individual MTs to run underneath and along the plasma membrane. MTs that pass over the T cell/APC interface are pulled by the dynein motors anchored at the IS cortex, causing the MTs to slide past the dynein while drawing the MTOC toward the IS. For a range of conditions, Kim and Maly (24) find that the cortical pulling mechanism is capable of reorienting the MTOC near the cell interface, and the misorientations of the MTOC were found to increase if the IS formed at a position near the location that is symmetrically opposite to the location of the T cell's MTOC. The inclusion of dynamic instability of the MTs in the model was found to have significant effects in improving the problem of misorientations.

More recently, Yi et al. (5) presented experimental evidence against the "cortical sliding" mechanism of MTOC relocation operating at the IS periphery and performed a series of experiments suggesting that the centrosome repositioning is driven by dynein by an "MT end-on capture-shrinkage" mechanism operating at the center of the IS. Using an optical trap, APCs were placed such that the initial contact point with the T cell appears exactly opposite to the location of the T cell's MTOC. Soon after the initiation of a successful contact, several MTs in T cell are observed to project from the MTOC, approaching toward the IS center by spontaneously bending along the cell outlet (as observed in Fig. 5 *A* of Yi et al. (5)), consistent with the previously observed MT structure in T cells (Fig. 6 *a* of Kuhn and Poenie (8)). Once the MTs' plus end reaches the IS center, dynein acts on it in an end-on fashion. The dynein power stroke then reels in the captured MTs that depolymerize ("shrink") when pulled against the IS cortex, which results in a movement of the MTOC toward the IS. A schematic visualization of this "MT end-on capture-shrinkage" mechanism of MTOC repositioning mediated by dynein is depicted in Fig. 1 a.

In contrast to the "cortical sliding" mechanism, in which all MTs tangential to the IS can potentially bind to dynein, the "MT end-on capture-shrinkage" mechanism necessitates the plus ends of MTs hitting a small area in the center of the IS and binding to dynein within. Here, we propose a stochastic "search and capture" model that assumes astral MTs grow and shrink rapidly in all directions from the MTOC, probing the inner surface of the plasma membrane until they capture a small dynein patch at the center of the IS. The remarkable concept of "search and capture" was first proposed in the context of mitotic spindle assembly after the discovery of the dynamic instability of MTs (25). Dynamic MTs nucleate from the MTOC, probing the cellular volume isotropically, and arrest the chromosome upon encounter with the kinetochore, a proteinous complex assembled at the centromeric region of the chromosomes (26,27). After several theoretical investigations (27–32), it was postulated that for an efficient search, 1) MTs' rescue frequency must be zero (i.e., MTs do not waste time searching in a direction missing the target) (28), and 2) catastrophe frequency is such that MTs grow on an average up to the target (i.e., MTs do not experience any early catastrophe while growing in the direction of the target) (28,29). In addition, several proposed mechanisms that can accelerate the search process include spatially biased MT growth toward the chromosomes (29,30,33), spatial arrangement of chromosome (30,34), kinetochore diffusion (28,30), interaction of MTs nucleated from kinetochore or/and chromosomes with the centrosomal MTs (26,30,35–37), augmin-promoted nucleation of MTs from the preexisting MTs and their interaction with centrosomal MTs (38,39), change in kinetochore architecture upon encountering MTs (40), and a recently observed "pivoting and search" mechanism, in which MTs pivot around the spindle pole in a random manner exploring the space laterally (26,41,42).

Although the term "search and capture" was first coined in the context of chromosome search during mitosis, the concept is very generic and fundamental for numerous cellular processes. MTs are the key regulator of the "search and capture" process and capture the target contact sites for successive cargo transport or to serve as ropes for the molecular motors on which they can sit and pull the MTs, facilitating a number of cellular functions such as nuclear migration in budding yeast (43), spindle positioning in *Caenorhabditis elegans* embryos (44), centrosome positioning in interphase cells (45,46), orientation of cortical MT array in plant cells (47), and nuclear positioning in fission yeast facilitated by the formation of parallel MT bundles (26,48). Moreover, in certain yeast species, such as *Cryptococcus neoformans*, MT-mediated capture and subsequent aggregation of the MTOCs organizes the premitotic assembly of spindle pole body (SPB) (49). Likewise, reassembly of Golgi via the concentrated effort of centrosomal MTs and the Golgi-driven MTs is also thought to rely on a "search and capture" hypothesis (50).

To initialize the reorientation of the T cell's MTOC toward the IS, the efficiency of the "search and capture" process is crucial. Any perturbations in the MT dynamics may cause severe delay in the MTOC relocation process (5). To estimate the efficiency of the search strategy, we calculate the time required by the MTs to bind to the dynein-enriched target at the central region of the IS (henceforth, synonymous with target). The faster the MTs find the target, the faster the MTOC can reorient and deliver various cargoes

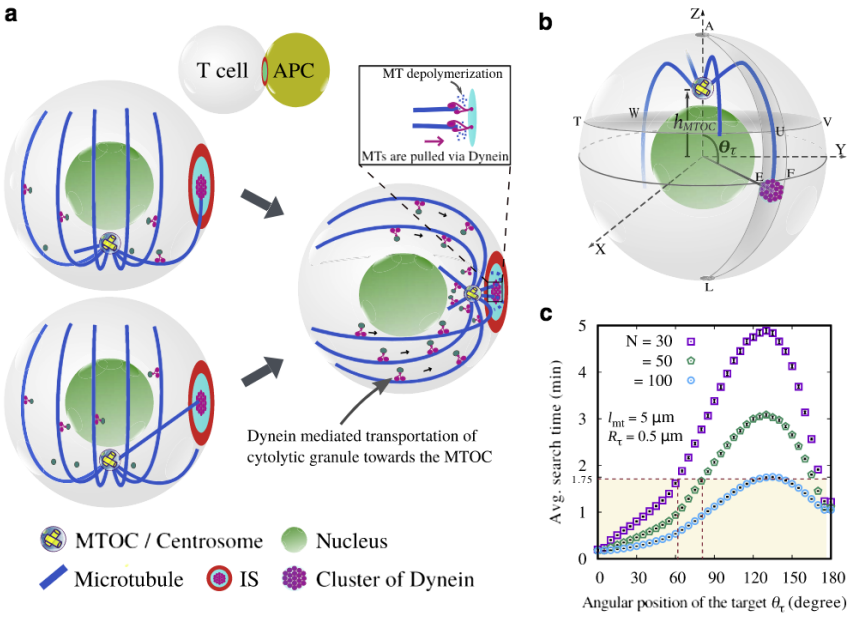


FIGURE 1 Schematics of the microtubule (MT)-mediated end-on capture of the target localized at the center of the immunological synapse (IS) in T cells initiating the MTOC relocation. (*a*) A sketch of MTOC relocation driven by the "MT-mediated end-on capture-shrinkage" mechanism (5) is shown. The T cell is represented by the outer sphere, the nucleus by the inner sphere, MTs are extending out from MTOC or Centrosome, and the target (a cluster of dynein) is the central disc within IS. Relocation of the MTOC near the IS occurs after the capture of MTs by the dynein motors localized in a patch at the IS center and subsequent development of the tension on the MTs by dynein and MT depolymerization acting in concert (see the *inset*). MTs can capture the target in two different ways: directly and/or by gliding along the cell periphery. (*b*) A sketch of the theoretical model demonstrating MTs growing from the MTOC in random directions and capturing the target upon encounter is shown. The MTOC is placed along the $z$ axis above the nucleus in a distance $h_{MTOC}$ from the cell center. The target is located on the cell periphery at an arbitrary polar angle $\theta_\tau$ (where $0^\circ \leq \theta_\tau \leq 180^\circ$) measured from the positive $z$ axis. For illustration, the target in this figure is positioned at a polar angle ~90°. The target located above the imaginary horizontal plane *TUVW* can be captured by the MTs directly and indirectly, whereas the target located below the plane is captured only indirectly. (*c*) Simulation results showing average search time as a function of the target polar angle $\theta_\tau$ with 30, 50, and 100 searching MTs are given. Notice that for 100 searching MTs, the search time is within 1.75 min, whereas for 30 and 50 searching MTs, the target is successfully captured within this timescale if the target is located below the polar angles 62 and 82°, respectively. Average search times maximize around $\theta_\tau = 132^\circ$. The model parameters are cell radius $R_C = 5$ $\mu$m, $h_{MTOC}$ = nuclear radius $R_N = 2.5$ $\mu$m, average MT length $l_{mt} = 5$ $\mu$m, and target radius $R_\tau = 0.5$ $\mu$m, and the MT dynamic instability parameters are growth velocity $v_g = 14.3$ $\mu$m/min, shrink velocity $v_s = 16$ $\mu$m/min, catastrophe frequency $f_c = v_g/l_{mt}$, and rescue frequency $f_r = 0$. The standard error of the mean is smaller than the corresponding point sizes. To view this figure in color, go online.

to the target site efficiently. We formulate a mathematical model for this process and show that for biologically relevant parameters of the process, the MT capture at the IS, and concomitantly the initiation of the MTOC relocation, is robustly achieved on timescales comparable to experimental measurements (5). Further, we developed a computational model using stochastic searching MTs, which confer additional support to the analysis and provide significant insights about the system. Utilizing the model, we could predict optimized values of the parameters corresponding to the minimal search time.

## METHODS

### Computational model

T cells under the conditions as in (5) have a spherical shape, with a radius of ~5–7 $\mu$m, and have a large spherical nucleus, leaving only a few-$\mu$m-thick shell for the cytoplasm and cytoskeleton, in particular for the MTOC and MTs. Therefore, we consider the cell and the nucleus as two concentric spheres centered at the origin of radii $R_C$ and $R_N$, respectively. The MTOC is placed along the $z$ axis above the north pole of the nucleus at $h_{MTOC}$ (the north pole of the nucleus is the point on the periphery of the nuclear envelope with $z = R_N$; see Fig. 1 b). The dynein-enriched target zone in the center of the IS is modeled as a circular stationary patch embedded on the cell periphery depicted in Fig. 1 b. MTs nucleate from the MTOC, grow and shrink rapidly while probing the space isotropically, and capture the target upon encounter. Each MT is considered as a rod of negligible thickness with the plus end growing at a constant velocity ($v_g$) until a catastrophe occurring at a frequency $f_c$. After a catastrophic event, the plus end of the MT shrinks with a constant velocity $v_s$. Upon rescue with a finite frequency $f_r$, MT grows again in the same direction, whereas the new cycle starts in a random direction if $f_r = 0$.

Statistically, the distance covered by the MT tip without undergoing a catastrophe is crucial to find the target placed on the cell periphery, indicating that the average search time is a function of the average MT length $l_{mt}$ and dynamical parameters. Earlier studies on "search and capture" of chromosomes (28–30) suggested that an efficient search would require the MT to explore the space randomly in all possible directions. Accordingly, upon completion of an unsuccessful attempt to capture the target, MTs should not be rescued. An optimal search, therefore, primarily requires setting the rescue frequency to zero ($f_r = 0$) and allowing the MTs to grow, on an average, up to the length $l_{mt}$ by regulating $f_c$ at a fixed $v_g$ through the relation $l_{mt} = v_g/f_c$ (see the Supporting Materials and Methods).

We study the MT dynamics by a stochastic model incorporating the four parameters ($v_g$, $v_s$, $f_c$, $f_r$) described earlier. The direction of the MT nucleated from the MTOC is described by a polar angle $\theta$ (where $\theta \in [0, \pi]$) and an azimuthal angle $\phi$ (where $\phi \in [0, 2\pi]$) in the standard spherical polar frame of reference. Depending on the direction of MT nucleation, two distinct scenarios arise: 1) an MT hits the nucleus and undergoes instantaneous catastrophe, leading to complete depolymerization and de novo nucleation of the MT in a random direction; and 2) the MT encounter with the cell periphery spontaneously curves along the cell surface, preferring the direction of minimal curvature. Before reaching the cell periphery, the MT remains straight. The MT is stabilized when the plus end makes a contact with the target, and the target is said to be captured. Our model hypothesis of spontaneous gliding of MTs along the cell periphery is based on the observed MT contours, where individual MTs projected from the MTOC appeared to glide along the cell periphery approaching the target

(5,8). Additionally, we also considered the effect of cell-boundary-induced catastrophe of the MTs, i.e., upon interacting with the cell wall, the MTs either undergo catastrophe or glide along the cell periphery, depending on the MT nucleation direction. Unless explicitly specified elsewhere, the results are reported without considering any perturbation of MT dynamics due to the interaction between cell wall and MT plus tip. Additional technical details of the computational model are presented in the Supporting Materials and Methods.

Unless otherwise specified, we simulated T cells with cell radius $R_C = 5\ \mu$m, nuclear radius $R_N = 2.5\ \mu$m, target radius $R_\tau = 0.5\ \mu$m, and the following MT dynamic instability parameters: growth velocity $v_g = 14.3\ \mu$m/min, shrink velocity $v_s = 16\ \mu$m/min, catastrophe frequency $f_c = v_g/l_{mt}$, and rescue frequency $f_r = 0$. The reference parameters and additional parameters around the reference value are recorded in Table S1.

## RESULTS AND DISCUSSION

### Unbiased search by dynamic MTs efficiently capture the target within experimentally relevant timescale

The central question of the stochastic search-and-capture process described by our model is whether such a random process can lead to the capture of one or more of the MTs at the IS in a few minutes. Before we present the results of our detailed mathematical model (Fig. S1), we estimate briefly the expected timescales based on a simplified picture. We assume that the T cell is spherical with radius $R_C = 5\ \mu$m, and, for simplicity, the MTOC is located somewhere immediately underneath the cell boundary. We identify the position of the MTOC with the north pole of the sphere and assume that the center of the target with radius $R_\tau = 0.5\ \mu$m is located on the surface of the sphere at a polar angle $\theta_\tau$ with respect to the north pole. T cells are small, so we can consider the simplistic scenario that there is not much space between the nucleus and the plasma membrane, and we can assume that MTs grow from the MTOC along the cell surface in a random direction. They grow on average to a length $l_{mt} \approx \pi R_C \approx 15\ \mu$m (i.e., from the north to the south pole) with a growth velocity $v_g \approx 15\ \mu$m/min (28) and then shrink with approximately the same speed $v_s$, unless they hit the target, where the plus end of the MT is immediately captured. In case the target is missed, the average time for an MT to grow and shrink again is $T_u = l_{mt}/v_g + l_{mt}/v_s \approx 2$ min; on completion of the cycle, the MT starts to grow in a new random direction. Thus, 2 min is the average timescale for an unsuccessful attempt of one MT to hit the target. The probability, $P_{direction}$, for a successful growth toward the target is the ratio between the diameter of the target ($2R_\tau = 1\ \mu$m) and the perimeter of the circle at the polar angle $\theta_\tau$, $L = 2\pi R_C \sin\theta_\tau$, provided $\theta_\tau$ is large. Note that this imaginary circle inscribed at latitude $\theta_\tau$ is parallel to the equatorial circle. Because $L$ is the largest for the equatorial positioning of the target ($\theta_\tau = \pi/2$), $P_{direction}$ will be larger than $R_\tau/\pi R_C \approx 0.032$ elsewhere. The average number of unsuccessful trials (i.e., MTs grow and shrink without hitting the target) is $N_u = 1/P_{direction} = \pi R_C/R_\tau \approx 31$ and takes about $T_{av} = N_u T_u = 62$ min. Consequently, a single dynamic MT needs, on the average, less than 62 min to hit the target; likewise, for $N$ dynamic MTs, the average time reduces to $T_{av}(N) = max\{T_{av}/N,\ R_C\theta_\tau/v_g\}$; thus, for several tens of MTs, the average capture time is just the time an MT needs to grow up to the target at polar angle $\theta_\tau$, i.e., less than 2 min. This estimate agrees well with the experimentally observed time between the formation of the IS and the start of the movement of the MTOC (5).

In the following, we support this estimate by extensive simulations of a detailed quantitative model described earlier. We place the IS at various locations on the periphery of the cell to estimate the average search time as a function of the target position. The MTOC is placed along the $z$ axis above the nuclear surface at a distance $h_{MTOC}$ measured from the center of the cell/nucleus. MTs nucleate from the MTOC and search for the target uniformly in all possible directions. In this model system, a single MT can capture the target in two different ways: 1) directly and 2) by gliding along the cell surface.

### Capture time is maximal for targets located near equatorial positions

We choose the experimentally relevant cell radius 5 $\mu$m (5) and nucleus radius 2.5 $\mu$m (51,52). We set the average MT length ($l_{mt}$), to be determined by the dynamic instability parameters of the MT (see Eqs. S1 and S2), to $l_{mt} = 5\ \mu$m, and we use the optimal zero rescue frequency (Fig. S2). In Fig. 1 c, we show the average search time as a function of the target polar angle. The maximal average capture time $\sim$1.75 min for 100 searching MTs is close to the experimental observation (5) and supported by the result of the scaling arguments discussed in the last section. When the number of MTs is reduced to 50 and 30, the target is successfully captured within the same time limit, provided the target polar angles does not exceed $\sim$82 and $\sim$62°, respectively. For $N = 50$, 30 MTs, the maximal capture times are $\sim$3 and $\sim$4.9, respectively (Fig. 1 c). Fig. 1 c shows that the mean search time as a function of target polar angle monotonically increases to a maximum and then falls off rapidly. The search time is minimal when the IS is formed at the proximal pole on the cell surface with respect to the MTOC (i.e., $\theta_\tau = 0°$). Interestingly, average search time increase only marginally when the target is located at the distal pole (i.e., $\theta_\tau = 180°$). The search time maximizes at an intermediate position of the target away from the poles.

In Fig. 2, a–c, we show the capture time of a single MT as a function of the angular position $\theta_\tau$ of the target for different cell and nucleus radii ($R_C$ and $R_N$), target radii ($R_\tau$), and average MT lengths ($l_{mt}$). We find that the search time decreases rapidly with increasing target size and that the variation is maximal when the target is localized around the equatorial periphery of the cell (i.e., $\theta_\tau = 90°$). Fig. 2 b shows that the capture time is significantly reduced in the smaller T cell.

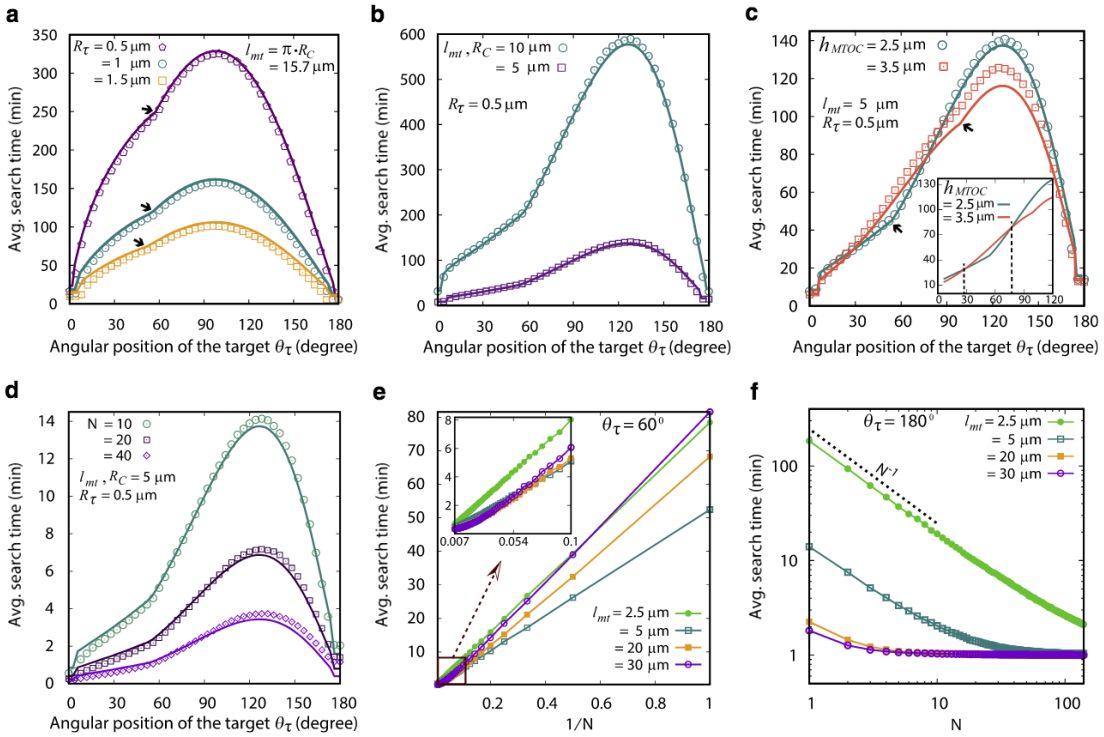


FIGURE 2 (*a–c*) Search time for a single MT varies with the angular position of the target $\theta_\tau$ for different parameters. The solid lines are from the analytical prediction, whereas the simulated data are shown by points. (*a*) Search times for cell radius $R_C = 10\ \mu$m, $h_{MTOC} = R_N = 5\mu$ m, and for varying target radii $R_\tau = 0.5$ , 1, and 1.5 $\mu$m are shown. The black arrow indicates a sudden increase in the average search time; see text. (*b*) Search times for two different cell sizes are shown: $R_C = 10\ \mu$m, $h_{MTOC} = R_N = 5\ \mu$m and $R_C = 5\ \mu$m, $h_{MTOC} = R_N = 2.5\ \mu$m. Average MT length $l_{mt} = R_C$ and target size $R_\tau = 0.5\ \mu$m. (*c*) Search times for different MTOC positions are shown: $R_\tau = 0.5\ \mu$m, $l_{mt} = R_C = 5\ \mu$m, and $R_N = 2.5\ \mu$m; search times are shown for $h_{MTOC} = 2.5\ \mu$m and $h_{MTOC} = 3.5\ \mu$m. Besides having characteristic similarities with (*a*) and (*b*), we find two crossovers in the average search time around $\theta_\tau = 30$ and 75° (shown in the *inset*). (*d–f*) Search time decreases with the number of MTs. Here, we have fixed $R_C = 5\ \mu$m, $h_{MTOC} = R_N = 2.5\ \mu$m, $R_\tau = 0.5\ \mu$m, and $f_c = v_g/l_{mt}$. (*d*) Search time as a function of the angular position of the target $\theta_\tau$ with number of searching MTs $N = 10$, 20, and 40 is shown. The solid lines are obtained from the analytical prediction, and the points represent the simulated value. (*e*) Search time is plotted against the inverse of the number of searching MTs (i.e., $1/N$), showing the time until capture decreases linearly with $1/N$ as the number of MTs increased. However, in the limit $N \gg 1$, the average search time deviates from the linear behavior (shown in the *inset*). (*f*) Average search time as a function of number of searching MTs ($N$) for different average length $l_{mt}$, in log-log scale, is shown. The target is placed at $\theta_\tau = 180°$. Notice that the average search time follows the inverse law (with $N$) indicated by the slope of the dotted reference line. To view this figure in color, go online.

Our simulation and analytically predicted data (see Supporting Materials and Methods for detailed analysis) independently predict the rise in the search time up to a certain angular position of the target reaching a maximum and then falling rapidly back to a value close to the initial one. A noticeable feature of the average search time profile is the kink at a specific polar angle of the target (indicated by *arrows* in Fig. 2 a). The feature appears when straight MT filaments directed toward the target are hindered by the nucleus and incidentally lose minimal visibility of the target required for the direct capture (i.e., target transit from above the imaginary tangential plane *TUVW* (Fig. 1 b) to below). Clearly, as long as the target is located above the imaginary tangential plane *TUVW*, it is fully visible to the MTs, implying that the MTs can directly capture the target (with probability $P_{direct,\tau\Uparrow}$; c.f. Supporting Materials and Methods). Once the target starts crossing the plane *TUVW* and becomes partially visible to the MTs, the direct capture probability ($P_{direct,\tau\overline{\Uparrow}}$; c.f. Supporting Materials and Methods) vanishes rapidly, leading to a sudden increase in the average capture time.

For longer MTs ($l_{mt} \gg R_C$), the search time becomes maximal at a polar angle $\theta_\tau \sim 90°$ of the target (Fig. 2 a). Here, the probability that the MT will be directed toward the target ($P_{direction}$) is minimal. For shorter MTs, the probability that the MT will survive (i.e., no catastrophe), $P_{no\ cat}$, is small whenever the polar angle of the target is large because the MT has to grow a long distance to find the target. Thus, the effect of $P_{no\ cat}$ becomes more significant, and the maximum of the average search time shifts toward larger polar angle $\theta_\tau$ of the target (Fig. 2 b).

## MTOC positioning within the cell significantly influences the capture time

The proximity of the MTOC to the cell periphery also significantly influences the capture time of the IS. Fig. 2 c demonstrates the variation of the average capture time as a

function of the target polar angle $\theta_\tau$ for two different MTOC locations: in the proximity of and away from the nuclear surface, quantified by the MTOC distances $h_{MTOC}$. The larger the $h_{MTOC}$ is, the closer the MTOC is to the membrane; thus, targets in the proximity (small target polar angles) and targets at the opposite side of the nucleus (large target polar angles, for which searching in the MTOC proximity is ineffective) can be found earlier. Fig. 2 c confirms this expectation and also shows that for intermediate angles, an MTOC position closer to the nucleus is more advantageous.

To understand MTOC position dependence on the capture time more quantitatively, we resort to the analytical calculation presented in the Supporting Materials and Methods. Essentially, the net capture probability is a sum of the probabilities of the MTs being capable of capturing the IS directly ($P_{direct}$) and the MTs having no direct access to the target but capable of searching by gliding along the cell surface (i.e., $P_{glide}$). Comparison of the two probabilities provides a clear picture of the underlying process and is described in Fig. S3. We notice that the simulation data deviate from our analytical predictions for the larger $h_{MTOC} = 3.5$ $\mu$m, i.e., when MTOC is relatively closer to the plasma membrane or farther away from the nuclear surface. A large separation between the MTOC and the nuclear surface allows the MTs to explore the space between them. Although the search remains unsuccessful because of the absence of IS in this region, the futile attempts by the MTs increases the average search time for capturing the target. The mathematical model presented here ignores this local search and hence deviates from the numerical data whenever MTOC is located away from the nuclear surface.

## Capture time depends on the number of searching MTs

Search time shortens if more than one MT participates in the search process (see Fig. 2, d–f). Fig. 2 d demonstrates the average search time as a function of the target polar angle for $N = 10$, 20, and 40 searching MTs. We find that the search time decreases linearly as $1/N$ (Fig. 2 e), which is again supported by our analytical considerations (see the Supporting Materials and Methods).

We further analyze this scenario by plotting the average search time as a function of the number of MTs for different target location ($\theta_\tau$). The search time tends to saturate beyond a certain number of MTs that depends on the average MT length. The saturation occurs earlier with longer average MT length $l_{mt}$ and with fewer MTs when the target is located at the distal pole of the cell (i.e., $\theta_\tau = 180°$) (Fig. 2 f). According to our analytical consideration elaborated in the Supporting Materials and Methods, the probability of a successful capture by $N$ number of MTs is $N$ times the probability of a successful search by a single MT, $P_c$. When $NP_c$ approaches 1, further increase of the number of MTs does not increase the capture probability anymore, and the search time as a function of $N$ saturates. For instance, in a cell with radius $R_C = 5$ $\mu$m, perinuclear MTOC ($h_{MTOC} = R_N = 2.5$ $\mu$m), average MT length $l_{mt} = 30$ $\mu$m, and target radius $R_\tau = 0.5$ $\mu$m located at the distant pole ($\theta_\tau = 180°$), two searching MTs ($N = 2$) yield $NP_c \sim 2 \times 0.6 = 1.2 \geq 1$ ($P_c$ is determined using Eq. S53), ensuring the capture process is purely deterministic.

## Optimized MT length minimize the average capture time for a small number of MTs

To explore the behavior of the search time with the average MT length ($l_{mt}$), the target is placed at a fixed polar angle $\theta_\tau = 60°$. The average search time is plotted as a function of the average MT length for different numbers of MTs in Fig. 3, a and b. Our data show that a single MT participating in the search process gives rise to a sharp minimum in the average search time for average MT length ~6 $\mu$m (i.e., $f_c \sim 2.38$ min$^{-1}$). This feature is characteristically very similar to the "search and capture" scenarios studied in the context of spindle assembly during mammalian mitosis (28–30). If the catastrophe frequency ($f_c$) is small, MTs waste time searching in the wrong directions; on the contrary, if the catastrophe frequency is large, MTs undergo premature catastrophe before reaching the target. Therefore, for an optimal search, $f_c$ (or $l_{mt}$) must be adjusted such that the MT grows just enough to reach the target. As the number of MTs increases, the minimum in the average search time becomes shallower for longer MTs (data not shown here) and finally vanishes for $N \gg 1$ (Fig. 3 b). In this limit, the effective search probability $NP_c$ that at least one MT (out of $N$ MTs) will be able to capture the target becomes very large, and hence the optimization feature is lost.

As expected, for the target localized near the south pole of the cell (i.e., $\theta_\tau \sim 180°$), MTs nucleated at any azimuthal angle $\phi$ will have a finite probability to capture the target. However, for a short MT, this probability is too small, causing the capture time to diverge. On the contrary, longer MTs can always find the target; thus, the sharp minimum in the average search time vanishes even when a single MT is executing the search (data not shown here). If the target is located near the north pole of the cell (i.e., $\theta_\tau \sim 0°$) and a single MT carries out the search, there are two possible ways the MT can progress: the MT captures the target directly or glides along the cell periphery and captures the target after a complete circle. For this specific position of the target, shorter MTs have a higher probability for direct capture; however, the capture probability diminishes if the direct capture fails and subsequently MTs glide along the cell periphery. Hence, we find a minimum in the average capture time if the average MT length $l_{mt}$ is close to the distance between the MTOC and the target (i.e., 2.5 $\mu$m). Further increase of the $l_{mt}$ increases the average capture

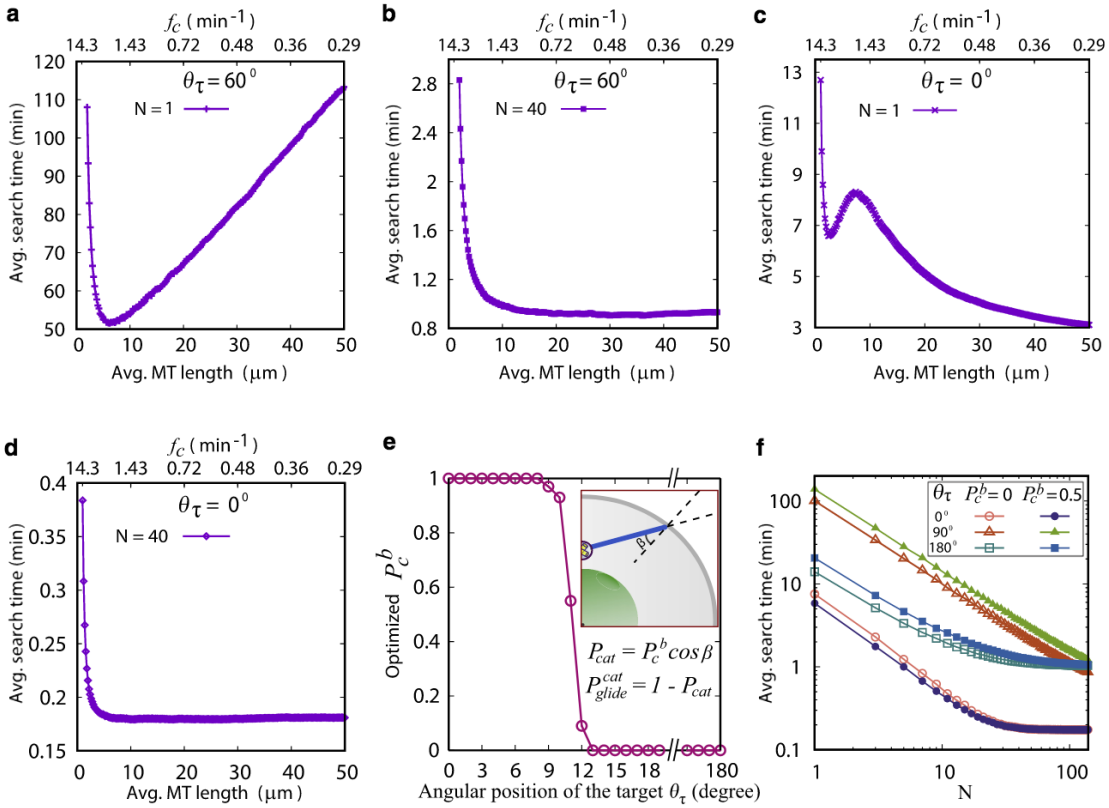


FIGURE 3 Search time as a function of the average MT length (*a–d*) and the effect of boundary-induced catastrophe of the MTs (*e* and *f*). Target is fixed at $\theta_\tau = 60°$ and $h_{MTOC} = 2.5$ μm. The upper *x* axis indicates the MT catastrophe frequency $f_c$ defining the average MT length. (*a*) Search time is shown as a function of average MT length $l_{mt}$ for $N = 1$, target is fixed at $\theta_\tau = 60°$. The minimum is at $l_{mt} \sim 6$ μm. (*b*) Same as (*a*) but for $N = 40$ is shown. The minimum vanished. (*c*) Same as (*a*) but with target fixed at $\theta_\tau = 0°$ is shown. The local minimum is at $l_{mt} \sim 2.5$ μm. (*d*) Same as in (*c*) but for $N = 40$ is shown. The minimum vanished. (*e*) Optimal probability parameter for boundary-induced MT catastrophe as a function of the target location ($\theta_\tau$) is shown. (*f*) Search time is shown as a function of the number of searching MTs for three different target positions, $\theta_\tau = 0$, 90, and 180°, and for two different probability parameters for boundary-induced MT catastrophe $P_c^b$, 0 and 0.5. To view this figure in color, go online.

time. For large $l_{mt}$, the probability of capturing the target along the cell periphery dominates, leading to a further decrease in the average capture time beyond a certain MT length (Fig. 3 c). In the limit in which the number of MTs is large ($N \gg 1$), we see a monotonic decrease in the search time (Fig. 3 d).

## Effect of boundary-induced catastrophe of MTs

Although in T cells, MTs emanating from the centrosome appear to follow the curvature of the plasma membrane toward the IS (c.f (5)), it has been observed in other cell lines that MTs impinging upon the plasma membrane either undergo catastrophe or continue to grow along the cell periphery (26,53,54). Several studies show that the distribution of the MTs along the cell periphery is determined by the cell shape, and the chances of the MTs to bend or undergo catastrophe upon interaction with the cell periphery are guided by the angle of incidence at the cell cortex (26,53,54). Therefore, we analyze in this section the effect of boundary-induced catastrophe upon the search process.

It appears plausible that MTs hitting the cell boundary nearly tangential at large angles of incidence (i.e., small angle between the cell periphery and the MT) are prone to glide along the cell periphery, and those hitting at small angles undergo rapid catastrophe. The catastrophe can also be enhanced by an opposing force at the MT plus end or by motor proteins such as kinesin-8 that do not depend on the angle of interaction (55,56). In the following, we consider only a probabilistic catastrophe induced by the cell boundary and depending on the MT's angle of incidence. Plausibly, the catastrophe probability $P_{cat}$ should depend on the angle ($\beta$) between the MT and the local normal vector of the plasma membrane. We therefore assume $P_{cat} = P_c^b \cos\beta$ and gliding probability as $P_{glide}^{cat} = 1 - P_{cat}$, where $P_c^b$ is the catastrophe probability parameter varied between 0 and 1 (see Supporting Materials and Methods). Consequently, upon interaction with the cell periphery, MTs undergo a catastrophe with zero probability for tangential incidence ($\beta = \pi/2$) and with probability $P_c^b$ for normal incidence (i.e., $\beta = 0$) (see *inset* of Fig. 3 e). Note that in the absence of boundary-induced catastrophe,

MTs spontaneously glide along the cell periphery, as considered earlier in this study.

In Fig. 3 e, we analyze the effect of the boundary-induced catastrophe of individual MTs on the average search time for different target location. The optimized value of $P_c^b$, which corresponds to the minimum of the average search time, is plotted as a function of target polar angle ($\theta_\tau$) for 10 searching MTs. We find that as long as the target remains in touch with the proximal pole of the cell with respect to the MTOC (north pole), the minimum in the average search time is obtained for $P_c^b = 1$. For this specific target positioning, MTs have a lesser chance to capture the target by gliding along the cell surface because the MTs having a smaller average length can rarely capture the target by traversing a complete circle around the cell periphery. The shorter MTs that grow steadily and capture the target directly dominate the capture process. In this case, $P_c^b = 1$ would prevent most of the MTs from gliding along the cell periphery, causing the emergence of a large number of shorter MTs that ultimately decrease the average search time by capturing the target directly. Strikingly, for the target located slightly away from the proximal pole (north pole), optimized $P_c^b$ decreases rapidly, and eventually for all large polar angles of the target ($\theta_\tau$), the minimum in the average search time is obtained with $P_c^b = 0$. For such target positioning, MTs that hit the cell periphery at polar angles smaller than the target location glide along the cell periphery toward the target, dominating the capture process.

Next, in Fig. 3 f, we plot the average search time as a function of the number of searching MTs for $P_c^b = 0.5$ and for the target positioned at $\theta_\tau = 0°$, $\theta_\tau = 90°$, and $\theta_\tau = 180°$, respectively. We compare these with the data obtained for $P_c^b = 0$ (i.e., no catastrophe upon interaction with the cell membrane). We find that for small numbers of MTs, the search times for catastrophe probability parameter $P_c^b = 0.5$ differ marginally from $P_c^b = 0$, whereas for a large number of MTs, the difference vanishes.

## Proper tuning of the MT parameters and the number of searching MTs lead to faster searching

In this section, we analyze how possible combinations of the relevant parameters affect quantitatively the efficiency of the capture process. First, we calculate the search time as a function of the average MT length $l_{mt}$ and the number of searching MTs $N$ for three different positions of the target on the cell periphery, viz., $\theta_\tau = 0°$ (north pole), 90° (equatorial plane), and 180° (south pole) (Fig. S4, *a–c*). For $\theta_\tau \sim 0°$, the target is found early (in $\lesssim$2 min) even with short MTs (Fig. S4 *a*). For the target located at $\theta_\tau = 90°$, the search takes longer if the number of MTs is small and a large number of MTs ($N \gtrsim 28$) is required to find the target in $\lesssim$2 min (Fig. S4 *b*). For a wide range of $N$ and $l_{mt}$, the average search time can be less than 2 min if the target is located at the south pole of the cell (i.e., $\theta_\tau = 180°$) (Fig. S4 *c*). Furthermore, the search time is reduced to ~1.03 min and ~0.83 min for $\theta_\tau = 180°$ with 10 searching MTs in a cell with $R_C = 5$ and 4 $\mu$m (52), respectively (Fig. S4 *d*).

Next, we analyze the variation of the search time with the MT growth velocity ($v_g$) at constant catastrophe frequencies (Fig. S5, *a–c*). The prevalent trend of the data indicates that the search time decreases rapidly with growth velocity and tends to saturate at large $v_g$. Capture time is reduced even further at smaller catastrophe frequencies with a large number of MTs (Fig. S5 *a*). Intuitively, one can correlate this with rapidly growing MTs searching the space relatively faster than sluggish MTs and the smaller catastrophe frequencies stabilizing the MTs growing in the direction of the target. However, the search carried out with a smaller number of MTs (e.g., $N = 10$) shows deviation from the monotonic decrease in the search time; a minimum in the average search time is observed as a function of $v_g$ at relatively lower catastrophe frequencies (Fig. S5 *b*). Clearly, with a few searching MTs, large $v_g$ and small catastrophe frequency ($f_c$) tend to increase the average MT length, and the MTs spend more time searching in the wrong direction. When the number of MTs becomes too large, the probability that at least one MT will move toward the target converges to unity, eliminating the optimization feature (Fig. S5 *a*). However, if the target is located at the distal pole (south pole) of the cell (i.e., $\theta_\tau = 180°$), the minimum in the average search time as a function of $v_g$ is not observed even with a small number of searching MTs (Fig. S5 *c*). The specific configuration facilitates the MT passing through the target location; therefore, small catastrophe frequencies and large growth velocities always lead to smaller search time. The effect of the MT shrink velocity ($v_s$) on the average search time (Fig. S5 *d*) is not substantial for a large number of MTs because $v_s$ does not affect the average MT length significantly. Nevertheless, the effect becomes significant for a small number of searching MTs because the higher the shrink velocity, the faster the MT can move back to the MTOC and grow afresh in another random direction looking for the target.

Another important parameter that can regulate the search time is the size of the nucleus. Depending on the target location on the cell periphery, the average search time decreases nonmonotonously with the increasing nuclear radius. Data suggest that if the target location is not directly accessible to the searching MTs because of steric hindrance from the nucleus (e.g., at $\theta_\tau = 90°$ in Fig. S5 *e*), the monotonous behavior is characteristically altered. The monotonous decrease in the average search time is due to the dominant effect of direct capture over the indirect capture, which is evident from the feature of the average search time for the target polar angle $\theta_\tau = 0°$. Because the target always remains visible to the MTs at this position, direct capture leads to the monotonous variation of the average search time for all values of the nuclear radius (Fig. S5 *e*). Clearly, the change occurs when the radius of the nucleus crosses

beyond a certain value for which the direct capture probability starts to diminish (see plot for $\theta_\tau = 60°$ in Fig. S5 *e*). Consistent with our expectations, the average search time is found to decrease with the target size (Fig. S5 *f*).

## CONCLUSIONS

Faithful reorientation of the T cell's MTOC toward the interface with the target cell is a prerequisite for the polarized secretion of the lytic granules containing perforin and granozymes at the target site, triggering the target cell lysis (5,7–12,57). Central to this, two mechanisms are thought to be involved in regulating the centrosome relocation. In the cortical sliding mechanism, dynein motors anchored at the periphery of the IS cortex reel in the MTs emanating from the centrosome, causing them to slide past the IS while drawing the centrosome toward the IS (8,22–24). Recently, Yi et al. (5) presented evidence favoring an "MT end-on capture-shrinkage" mechanism of MTOC repositioning, in which dyneins localized at the IS center interact with the MT's plus end in an end-on fashion so as to couple the MT's depolymerization with the movement of the MTOC toward the IS. According to the capture-shrinkage mechanism (5), the force generators (e.g., dyneins) are thought to localize at the center of the IS but not at the IS periphery, as was perceived earlier in the cortical sliding mechanism. Invagination of the T cell membrane at the center of the IS toward the MTOC, observed in "frustrated" T cell/APC conjugates where the MTOC is stuck behind the nucleus, clearly argued that the force generation mechanism is focused at the IS center. Additionally, dynamical imaging of the MTs during normal repositioning showed an MT end-on capture shrinkage operating at the IS center.

Our study addressed the question of effectiveness of this dynein-mediated "capture-shrinkage mechanism" in the light of a "search and capture" model in which individual MTs, nucleated from the MTOC, undergo dynamic instability until they are captured by dynein anchored at the IS cortex. We combined mathematical and numerical analyses to estimate the average time taken by the aster of MTs to secure an end-on attachment with dynein. Exponentially distributed time until capturing the target, obtained numerically, is conceived as an input conjecture for the mathematical model (Fig. S6). We find that the capture of the target is essentially a combination of a direct and an indirect process: direct capture occurs when MTs hit the target without prior interaction with the cell or nucleus—this process is prevalent for a target located in the cell hemisphere containing the MTOC—and indirect capture arises because of MTs that miss the target directly but glide along the cell surface seeking the target—this process is dominant in both the cell hemispheres and is the only mechanism of capture in the hemisphere lacking the MTOC.

We observed, in general, that the search time largely depends on the relative size of the cell and the nucleus; e.g., the search process becomes efficient upon reduction of the T cell diameter. The average search time for various locations of the IS on the cell periphery suggests that a single MT would rapidly capture the target located near the proximal or the distal poles of the cell. Away from the polar regions, capture time increases and maximizes at an intermediate angle determined by the system parameters. The monotonic increase in the capture time transit through a sudden jump away from the proximal pole occurs when the chance of directly capturing the target diminishes.

Although the target is rapidly captured at the distal pole, such positioning of the target might lead to a tug-of-war-like scenario during the MTOC relocation process. According to the observation of Kim and Maly (24) and others (58), the MTOC is sometimes stuck for a long time behind the nucleus for this specific target positioning. Because of the symmetry of the MT array nucleated from the MTOC, the target can be reached by the MTs from all directions at the same time, resulting in a vanishing dynein mediated net pull applied on the MTOC. The pulling forces toward the IS are so symmetrically distributed that to create an imbalance in the forces, which is required to translocate the MTOC toward the IS, a long delay may occur. Interestingly, Yi et al. (5) showed that in such a "frustrated" condition, the membrane of the IS center often invaginates to reach the stuck MTOC, demonstrating that the IS membrane can also move to the MTOC instead of the MTOC coming to the IS.

During IS formation, the centrosomes often appear to be dissociated from the nucleus both in migrating and in resting T cells (59), whereas in most other cell types, the centrosomes remain closely associated with the nuclear membrane through nesprins, a family of transmembrane proteins residing on the nuclear surface (60,61). Lui-Roberts et al. (59) showed that T cells in which centrosomes were irreversibly "glued" to the nucleus by expressing GFP-BICD2-NT-nesprin-3 were still able to kill the target after successful migration of their centrosome toward the IS. Naturally, the question arises why the position of the centrosomes varies in T cells. Lui-Roberts et al. (59) speculated that the dynamic centrosome positioning might help the migrating cells to jiggle around, seeking for the target cell. However, why the centrosomes in resting cells adopt different positions during IS formation has remained enigmatic. One possibility could be that the cell attempts to alter the search strategy that might be linked with the location of the target because our study suggests that distance of the MTOC from the nuclear surface significantly alters the capture time. Depending on the MTOC position above the nucleus, efficiency of the capture process varies for various angular position of the target along the cell surface. Interestingly, the average search times for the MTOC located proximal to the nucleus and away (close to the cell membrane) cross each other at two distinct angular positions of the target (see Fig. 2 c). Moreover, the MT array from the distant

MTOC is found to be more efficient in capturing the IS at small polar angles. For intermediate angular positions of the IS, MTs from the MTOC proximal to the nucleus are more effective, whereas MTs from the distant MTOC capture the large-angle targets relatively early. Analyzing the dependency of the average search time on the MTOC position, we argue that a T cell's MTOC may adopt different locations largely to optimize the time required to capture the target.

According to our analysis, the average search time decreases with the number of searching MTs and saturates beyond a certain number of MTs that depends on the position of the IS and the average MT length. Because all MTs search in parallel, the efficiency of the search process increases with the number of MTs. When a single MT carries out the search, an optimized value of the average MT length (or the catastrophe frequency) appears that corresponds to the minimum of the average search time. Interestingly, the optimization feature as a function of the average MT length diminishes if the number of MTs is very large. However, if the IS formed at the distal pole of the cell, the sharp minimum in the average capture time does not appear even in the context of a single searching MT. Because the average MT length is controlled by the growth velocity and catastrophe frequency, a minimum in the average search time as a function of the growth velocity appears at smaller catastrophe frequencies with a fewer searchers. A similar optimization feature at smaller catastrophe frequencies is not found with a large number of MTs; instead, a higher growth velocity, together with smaller catastrophe frequency, leads to a rapid capture. Capture time drops monotonically and does not pass through a minimum for the target located at the distal pole of the cell, even if the number of searching MTs is small. A similar type of feature is also observed in the context of kinetochore capture in fission yeast, in which the efficiency of the capture process is primarily determined by the average MT length (42). Because the catastrophe frequency and the growth velocity primarily control the average MT length, these parameters largely influence the capture process. A tabular list of the different capture time scenarios depending on the number of searching MTs and the target location is shown in Table 1.

Based on this observation, we argue that optimization in the average search time is a robust mechanism that leads to the rapid capture of the target and is therefore a prerequisite with fewer searchers. However, the optimization is not essential if the system contains a large number of MTs. Consequently, the set of fewer MTs also needs to be more dynamic to capture the target rapidly, whereas the search becomes faster with a large number of MTs when they are stable. Analysis of the average search time suggests that larger targets reduce the capture time. Search time also changes with the size of the nucleus. With increasing nuclear radius, average search time decreases nonmonotonically for targets with no direct capture possibility; for targets visible to the MTs before hitting the cell periphery, direct capture probability dominates over the indirect capture, resulting in a monotonous decrease in the average search time with nuclear size.

It is very likely that the cell and the nucleus could be different from a sphere; therefore, an extension of the current approach could include the analysis of capture efficiency considering aspherical architecture of cell and nucleus. In fact, it would be interesting to consider a spheroidal cell with the MTOC placed along its major/minor axis. Efficiency of the MTs capturing the target would depend on the specific positioning of the MTOC inside the cell. Similarly, the nucleus can also take a spheroidal shape. Because the nucleus acts as a steric hindrance for the MTs growing straightforwardly toward the target, the capture time would clearly depend on the angular position of the MTOC and the target. Besides, off-centered positioning of nucleus in the current model could also be relevant and more realistic. The nucleus, by being positioned away from the center of the cell, can regulate the capture time by increasing or decreasing the effective distance between the target and the perinuclear MTOC.

**TABLE 1 Average Search Time for Various Capture Scenarios Depending on the Number of Searching MTs and the Target Positions**

| | Target Position with Respect to MTOC ($\theta_\tau$) | | |
|---|---|---|---|
| Number of Searching MTs | Proximal (∼0–10°) | Intermediate (∼10–170°) | Distal (∼170–180°) |
| Single MT | Average search time is relatively small; a sharp minimum in the average search time observed as a function of average MT length. | Average search time is relatively large; a sharp minimum in the average search time observed as a function of average MT length. | Average search time is small; no minima in the average search time is obtained as a function of average MT length. |
| Few MTs (∼10) | Average search time is smaller than a single MT; minimum in the average search time persists, though becomes shallower. | Average search time is smaller than a single MT; minimum in the average search time persists, though becomes shallower. | Average search time is smaller than a single MT; no minima observed as a function of average MT length. |
| Many MTs (∼100) | Average search time is very small (∼0.2 min); no minima observed as a function of average MT length. | Average search time is small ($\lesssim$2 min); no minima observed as a function of average MT length. | Average search time is small (∼1 min); no minima observed as a function of average MT length. |

Although we have developed the model to understand the optimal search strategy in T cell, the model itself is more general. Most importantly, our model can be used to understand search processes in which direct as well as indirect search guided by the topology of the gliding surface on a curved manifold is significant. In fact, in the premitotic assembly of the central pole body (SPB) in yeast (*C. neoformans*) via MT-mediated capture and aggregation of MTOCs, this model can be extended to estimate the time required to form an SPB. In future, it would also be interesting to generalize the model to predict the mitotic assembly time, with emphasis on the recently explored MT features. Moreover, our model can be used directly or can be modified in a context-dependent manner to elucidate the efficiency of search strategies that crucially regulate many cellular functions in various organisms.

Certain aspects of our model motivate further experiments. It appears that the MT must glide along the plasma membrane to obtain the MT cytoskeleton organization referred to in (5), but a systematic study observing the dynamics of MTs growing along the plasma membrane in T cells remains to be done. We analyzed potential boundary-induced MT catastrophe in a phenomenological way by introducing a hitting-angle-dependent catastrophe probability and found that boundary-induced MT catastrophe even has an advantageous effect for small target angles and only mild effects for large target angles. For a better microscopic understanding, the gliding of MTs along the plasma membrane while one end is clamped at the MTOC raises two major concerns: 1) whether the MTs have sufficient resistance to bend without disintegrating the MT lattice. Previous studies suggest that the MTs have mechanical properties analogous to plexiglass and rigid plastics (62), and the yield strength of MTs is similar to that of polymethylmethacrylate (i.e., 40–70 MPa) (63); with a 25 nm diameter, they are sufficient enough to bend along the plasma membrane bearing the tensile load applied to it (24). Strikingly, recent studies by Schaedel et al. (64) showed that MTs that were damaged over extensive load might recover their initial stiffness by incorporating tubulin dimer into their lattice; 2) whether the MT catastrophe upon hitting the plasma membrane is biochemically suppressed or whether, for instance, vimentin filaments induce the increased curvature of MTs in the T cell. The MT plus-end tracking proteins (+TIPs) are well known for their ability to accumulate at the MT plus end and could modulate the MT dynamics. The most conserved +TIPs are the end-binding proteins (EBs), which may either interact directly with the MT plus end or in combination with other +TIPs (e.g., cytoplasmic dynein, dynactin, CLIP-170, $p150^{Glued}$, etc.) (65). An observation made in the mammalian cells by Komarova et al. (66) showed that EBs (particularly EB1 and EB2) have little effect on MT rescue but actively suppress the MT catastrophe. The observation of Komarova et al. (66) is in line with the observed anticatastrophe activity promoted by the proper homologs of mammalian EBs in fission yeast (67) and in *Xenopus* extracts (68). In addition, the intermediate filament vimentin (VIF), regarded as a long-lived copy of the MT filaments, could also regulate the MT dynamics via interacting with the MT through several proteins (69,70). It is observed that the motile cells like fibroblasts and lymphocytes have higher VIF levels (71), and recently, Gan et al. (72) showed that VIF could increase the persistence of the MTs to enhance the directed cell migration. Likewise, other cytoskeleton proteins, such as stable F-actin structures, could also guide MT organization. Similar experiments in T cells could provide a clear picture of the underlying mechanism of MT growth along the plasma membrane in T cells. It would also be crucial to identify the characteristics of dynein's cortical activities at the IS center (5) and the molecular basis of the bond formation between the MT plus end and the dynein.

## SUPPORTING MATERIAL

Supporting Material can be found online at https://doi.org/10.1016/j.bpj.2019.04.008.

## AUTHOR CONTRIBUTIONS

R.P. and H.R. designed the research. A.S. carried out all simulations and analyzed the data. R.P., A.S., and H.R. wrote the article.

## ACKNOWLEDGMENTS

R.P. acknowledges grant no. EMR/2017/001346 of the Science and Engineering Research Board, Department of Science and Technology, India for the computational facility. This work was financially supported by the German Research Foundation within the Collaborative Research Center SFB 1027 (H.R.), and R.P. acknowledges the SFB 1027 for supporting his visit to the Saarland University for discussion and finalizing the project. A.S.'s fellowship was supported by the University Grants Commission, India.

## SUPPORTING CITATIONS

References (73–77) appear in the Supporting Material.

## REFERENCES

1. Huang, Y., D. D. Norton, …, R. L. Wange. 2005. Deficiency of ADAP/Fyb/SLAP-130 destabilizes SKAP55 in Jurkat T cells. *J. Biol. Chem.* 280:23576–23583.
2. André, P., A. M. Benoliel, …, P. Bongrand. 1990. Use of conjugates made between a cytolytic T cell clone and target cells to study the redistribution of membrane molecules in cell contact areas. *J. Cell Sci.* 97:335–347.
3. Dustin, M. L., A. K. Chakraborty, and A. Shaw. 2010. Understanding the Structure and Function of the Immunological Synapse. *Cold Spring Harb. Perspect. Biol.* 2:a002311.
4. Monks, C. R., B. A. Freiberg, …, A. Kupfer. 1998. Three-dimensional segregation of supramolecular activation clusters in T cells. *Nature.* 395:82–86.

5. Yi, J., X. Wu, …, J. A. Hammer. 2013. Centrosome repositioning in T cells is biphasic and driven by microtubule end-on capture-shrinkage. *J. Cell Biol.* 202:779–792.
6. Hui, K. L., and A. Upadhyaya. 2017. Dynamic microtubules regulate cellular contractility during T-cell activation. *Proc. Natl. Acad. Sci. USA.* 114:E4175–E4183.
7. Schatten, H. 2011. The Centrosome: Cell and Molecular Mechanisms of Functions and Dysfunctions in Disease. Humana Press, New York.
8. Kuhn, J. R., and M. Poenie. 2002. Dynamic polarization of the microtubule cytoskeleton during CTL-mediated killing. *Immunity.* 16:111–121.
9. Kupfer, A., and G. Dennert. 1984. Reorientation of the microtubule-organizing center and the Golgi apparatus in cloned cytotoxic lymphocytes triggered by binding to lysable target cells. *J. Immunol.* 133: 2762–2766.
10. Yannelli, J. R., J. A. Sullivan, …, V. H. Engelhard. 1986. Reorientation and fusion of cytotoxic T lymphocyte granules after interaction with target cells as determined by high resolution cinemicrography. *J. Immunol.* 136:377–382.
11. Pasternack, M. S., C. R. Verret, …, H. N. Eisen. 1986. Serine esterase in cytolytic T lymphocytes. *Nature.* 322:740–743.
12. Krzewski, K., and J. E. Coligan. 2012. Human NK cell lytic granules and regulation of their exocytosis. *Front. Immunol.* 3:335.
13. Geiger, B., D. Rosen, and G. Berke. 1982. Spatial relationships of microtubule-organizing centers and the contact area of cytotoxic T lymphocytes and target cells. *J. Cell Biol.* 95:137–143.
14. Stinchcombe, J. C., E. Majorovits, …, G. M. Griffiths. 2006. Centrosome polarization delivers secretory granules to the immunological synapse. *Nature.* 443:462–465.
15. Kuhn, J. R., Z. Wu, and M. Poenie. 2001. Modulated polarization microscopy: a promising new approach to visualizing cytoskeletal dynamics in living cells. *Biophys. J.* 80:972–985.
16. Fukata, M., T. Watanabe, …, K. Kaibuchi. 2002. Rac1 and Cdc42 capture microtubules through IQGAP1 and CLIP-170. *Cell.* 109:873–885.
17. Watanabe, T., S. Wang, …, K. Kaibuchi. 2004. Interaction with IQGAP1 links APC to Rac1, Cdc42, and actin filaments during cell polarization and migration. *Dev. Cell.* 7:871–883.
18. Banerjee, P. P., R. Pandey, …, J. S. Orange. 2007. Cdc42-interacting protein-4 functionally links actin and microtubule networks at the cytolytic NK cell immunological synapse. *J. Exp. Med.* 204:2305–2320.
19. Lansbergen, G., and A. Akhmanova. 2006. Microtubule plus end: a hub of cellular activities. *Traffic.* 7:499–507.
20. Kuroda, S., M. Fukata, …, K. Kaibuchi. 1996. Identification of IQGAP as a putative target for the small GTPases, Cdc42 and Rac1. *J. Biol. Chem.* 271:23363–23367.
21. Bunnell, S. C., V. Kapoor, …, L. E. Samelson. 2001. Dynamic actin polymerization drives T cell receptor-induced spreading: a role for the signal transduction adaptor LAT. *Immunity.* 14:315–329.
22. Combs, J., S. J. Kim, …, M. Poenie. 2006. Recruitment of dynein to the Jurkat immunological synapse. *Proc. Natl. Acad. Sci. USA.* 103:14883–14888.
23. Stinchcombe, J. C., and G. M. Griffiths. 2014. Communication, the centrosome and the immunological synapse. *Philos. Trans. R. Soc. Lond. B Biol. Sci.* 369:20130463.
24. Kim, M. J., and I. V. Maly. 2009. Deterministic mechanical model of T-killer cell polarization reproduces the wandering of aim between simultaneously engaged targets. *PLoS Comput. Biol.* 5:e1000260.
25. Mitchison, T., and M. Kirschner. 1984. Dynamic instability of microtubule growth. *Nature.* 312:237–242.
26. Pavin, N., and I. M. Tolić-Nørrelykke. 2014. Swinging a sword: how microtubules search for their targets. *Syst. Synth. Biol.* 8:179–186.
27. Hill, T. L. 1985. Theoretical problems related to the attachment of microtubules to kinetochores. *Proc. Natl. Acad. Sci. USA.* 82:4404–4408.
28. Holy, T. E., and S. Leibler. 1994. Dynamic instability of microtubules as an efficient way to search in space. *Proc. Natl. Acad. Sci. USA.* 91:5682–5685.
29. Wollman, R., E. N. Cytrynbaum, …, A. Mogilner. 2005. Efficient chromosome capture requires a bias in the 'search-and-capture' process during mitotic-spindle assembly. *Curr. Biol.* 15:828–832.
30. Paul, R., R. Wollman, …, A. Mogilner. 2009. Computer simulations predict that chromosome movements and rotations accelerate mitotic spindle assembly without compromising accuracy. *Proc. Natl. Acad. Sci. USA.* 106:15708–15713.
31. Gopalakrishnan, M., and B. S. Govindan. 2011. A first-passage-time theory for search and capture of chromosomes by microtubules in mitosis. *Bull. Math. Biol.* 73:2483–2506.
32. Mulder, B. M. 2012. Microtubules interacting with a boundary: mean length and mean first-passage times. *Phys. Rev. E Stat. Nonlin. Soft Matter Phys.* 86:011902.
33. Carazo-Salas, R. E., G. Guarguaglini, …, I. W. Mattaj. 1999. Generation of GTP-bound Ran by RCC1 is required for chromatin-induced mitotic spindle formation. *Nature.* 400:178–181.
34. Magidson, V., C. B. O'Connell, …, A. Khodjakov. 2011. The spatial arrangement of chromosomes during prometaphase facilitates spindle assembly. *Cell.* 146:555–567.
35. Kitamura, E., K. Tanaka, …, T. U. Tanaka. 2010. Kinetochores generate microtubules with distal plus ends: their roles and limited lifetime in mitosis. *Dev. Cell.* 18:248–259.
36. Karsenti, E., J. Newport, and M. Kirschner. 1984. Respective roles of centrosomes and chromatin in the conversion of microtubule arrays from interphase to metaphase. *J. Cell Biol.* 99:47s–54s.
37. Sikirzhytski, V., V. Magidson, …, A. Khodjakov. 2014. Direct kinetochore-spindle pole connections are not required for chromosome segregation. *J. Cell Biol.* 206:231–243.
38. Petry, S., A. C. Groen, …, R. D. Vale. 2013. Branching microtubule nucleation in Xenopus egg extracts mediated by augmin and TPX2. *Cell.* 152:768–777.
39. Sánchez-Huertas, C., and J. Lüders. 2015. The augmin connection in the geometry of microtubule networks. *Curr. Biol.* 25:R294–R299.
40. Magidson, V., R. Paul, …, A. Khodjakov. 2015. Adaptive changes in the kinetochore architecture facilitate proper spindle assembly. *Nat. Cell Biol.* 17:1134–1144.
41. Kalinina, I., A. Nandi, …, I. M. Tolić-Nørrelykke. 2013. Pivoting of microtubules around the spindle pole accelerates kinetochore capture. *Nat. Cell Biol.* 15:82–87.
42. Blackwell, R., O. Sweezy-Schindler, …, M. D. Betterton. 2017. Contributions of microtubule dynamic instability and rotational diffusion to kinetochore capture. *Biophys. J.* 112:552–563.
43. Adames, N. R., and J. A. Cooper. 2000. Microtubule interactions with the cell cortex causing nuclear movements in Saccharomyces cerevisiae. *J. Cell Biol.* 149:863–874.
44. Grill, S. W., J. Howard, …, A. A. Hyman. 2003. The distribution of active force generators controls mitotic spindle position. *Science.* 301:518–521.
45. Som, S., S. Chatterjee, and R. Paul. 2019. Mechanistic three-dimensional model to study centrosome positioning in the interphase cell. *Phys. Rev. E.* 99:012409.
46. Zhu, J., A. Burakov, …, A. Mogilner. 2010. Finding the cell center by a balance of dynein and myosin pulling and microtubule pushing: a computational study. *Mol. Biol. Cell.* 21:4418–4427.
47. Ambrose, C., J. F. Allard, …, G. O. Wasteneys. 2011. A CLASP-modulated cell edge barrier mechanism drives cell-wide cortical microtubule organization in Arabidopsis. *Nat. Commun.* 2:430.
48. Tran, P. T., L. Marsh, …, F. Chang. 2001. A mechanism for nuclear positioning in fission yeast based on microtubule pushing. *J. Cell Biol.* 153:397–411.
49. Sutradhar, S., V. Yadav, …, K. Sanyal. 2015. A comprehensive model to predict mitotic division in budding yeasts. *Mol. Biol. Cell.* 26:3954–3965.

50. Vinogradova, T., R. Paul, …, I. Kaverina. 2012. Concerted effort of centrosomal and Golgi-derived microtubules is required for proper Golgi complex assembly but not for maintenance. *Mol. Biol. Cell.* 23:820–833.

51. Peglow, M., B. A. Niemeyer, …, H. Rieger. 2013. A calcium-redox feedback loop controls human monocyte immune responses: the role of ORAI Ca2+ channels. *New J. Phys.* 15:055022.

52. Maccari, I., R. Zhao, …, H. Rieger. 2016. Cytoskeleton rotation relocates mitochondria to the immunological synapse and increases calcium signals. *Cell Calcium.* 60:309–321.

53. Picone, R., X. Ren, …, B. Baum. 2010. A polarised population of dynamic microtubules mediates homeostatic length control in animal cells. *PLoS Biol.* 8:e1000542.

54. Laan, L., N. Pavin, …, M. Dogterom. 2012. Cortical dynein controls microtubule dynamics to generate pulling forces that position microtubule asters. *Cell.* 148:502–514.

55. Foethke, D., T. Makushok, …, F. Nédélec. 2009. Force- and length-dependent catastrophe activities explain interphase microtubule organization in fission yeast. *Mol. Syst. Biol.* 5:241.

56. Varga, V., C. Leduc, …, J. Howard. 2009. Kinesin-8 motors act cooperatively to mediate length-dependent microtubule depolymerization. *Cell.* 138:1174–1183.

57. Kupfer, A., S. J. Singer, and G. Dennert. 1986. On the mechanism of unidirectional killing in mixtures of two cytotoxic T lymphocytes. Unidirectional polarization of cytoplasmic organelles and the membrane-associated cytoskeleton in the effector cell. *J. Exp. Med.* 163:489–498.

58. Serrador, J. M., M. Nieto, and F. Sánchez-Madrid. 1999. Cytoskeletal rearrangement during migration and activation of T lymphocytes. *Trends Cell Biol.* 9:228–233.

59. Lui-Roberts, W. W., J. C. Stinchcombe, …, G. M. Griffiths. 2012. Cytotoxic T lymphocyte effector function is independent of nucleus-centrosome dissociation. *Eur. J. Immunol.* 42:2132–2141.

60. Malone, C. J., L. Misner, …, J. G. White. 2003. The C. elegans hook protein, ZYG-12, mediates the essential attachment between the centrosome and nucleus. *Cell.* 115:825–836.

61. Schneider, M., W. Lu, …, I. Karakesisoglou. 2011. Molecular mechanisms of centrosome and cytoskeleton anchorage at the nuclear envelope. *Cell. Mol. Life Sci.* 68:1593–1610.

62. Gittes, F., B. Mickey, …, J. Howard. 1993. Flexural rigidity of microtubules and actin filaments measured from thermal fluctuations in shape. *J. Cell Biol.* 120:923–934.

63. Botvinick, E. L., V. Venugopalan, …, M. W. Berns. 2004. Controlled ablation of microtubules using a picosecond laser. *Biophys. J.* 87:4203–4212.

64. Schaedel, L., K. John, …, M. Théry. 2015. Microtubules self-repair in response to mechanical stress. *Nat. Mater.* 14:1156–1163.

65. Wu, X., X. Xiang, and J. A. Hammer, III. 2006. Motor proteins at the microtubule plus-end. *Trends Cell Biol.* 16:135–143.

66. Komarova, Y., C. O. De Groot, …, A. Akhmanova. 2009. Mammalian end binding proteins control persistent microtubule growth. *J. Cell Biol.* 184:691–706.

67. Busch, K. E., and D. Brunner. 2004. The microtubule plus end-tracking proteins mal3p and tip1p cooperate for cell-end targeting of interphase microtubules. *Curr. Biol.* 14:548–559.

68. Tirnauer, J. S., S. Grego, …, T. J. Mitchison. 2002. EB1-microtubule interactions in Xenopus egg extracts: role of EB1 in microtubule stabilization and mechanisms of targeting to microtubules. *Mol. Biol. Cell.* 13:3614–3626.

69. Prahlad, V., M. Yoon, …, R. D. Goldman. 1998. Rapid movements of vimentin on microtubule tracks: kinesin-dependent assembly of intermediate filament networks. *J. Cell. Biol.* 143:159–170.

70. Huber, F., A. Boire, …, G. H. Koenderink. 2015. Cytoskeletal crosstalk: when three different personalities team up. *Curr. Opin. Cell Biol.* 32:39–47.

71. Mendez, M. G., S. Kojima, and R. D. Goldman. 2010. Vimentin induces changes in cell shape, motility, and adhesion during the epithelial to mesenchymal transition. *FASEB J.* 24:1838–1851.

72. Gan, Z., L. Ding, …, G. Danuser. 2016. Vimentin intermediate filaments template microtubule networks to enhance persistence in cell polarity and directed migration. *Cell Syst.* 3:252–263.e8.

73. Verde, F., M. Dogterom, …, S. Leibler. 1992. Control of microtubule dynamics and length by cyclin A- and cyclin B-dependent kinases in Xenopus egg extracts. *J. Cell Biol.* 118:1097–1108.

74. Dogterom, M., and S. Leibler. 1993. Physical aspects of the growth and regulation of microtubule structures. *Phys. Rev. Lett.* 70:1347–1350.

75. Sokolnikoff, I., and R. Redheffer. 1966. Mathematics of Physics and Modern Engineering. McGraw-Hill, New York.

76. Todhunter, I. 1886. Spherical Trigonometry: For the Use of Colleges and Schools. MACMILLAN AND CO, London, UK.

77. Ross, S. 1972. Introduction to Probability Models. Academic Press, New York.